Chapter 10
Reliability and Correlation Analysis of Computed Methods to Convert Conventional 2D Radiological Hindfoot Measurements to 3D Equivalents Using Weight Bearing CT

Introduction

Exact radiographic assessment of hindfoot alignment remains a challenge [1, 2]. The various measurement techniques and hindfoot views (either inclined anteroposterior (AP) or posterioranterior (PA)) reflect the lack of a standardized and accurate methodology [3]. All current methodologies try to overcome two main inaccuracies: the superposition caused by the osseous structures in the midfoot and the rotational errors created during the positioning of the foot, as demonstrated by several recent studies [4–6]. Weight bearing CT (WBCT) of the foot and ankle has been shown to be more accurate in hindfoot measurements [7]. This recent imaging technique offers the advantage of a standing position as with weight bearing radiographs but overcomes the disadvantages of the osseous superposition caused by the complex anatomy of the foot and ankle [8–10]. This allows for complete visualization of the hindfoot [11]. Additionally, WBCT software settings can rotate the foot and ankle after the imaging process to acquire a standardized positioning of the hindfoot [7, 8].

Although computed tomography was introduced to orthopedic surgery in the mid-1970s [12], its routine clinical and 3D use only started in the early 1990s with the introduction of the spiral CT, which allowed better insight into complex fracture patterns [13]. Further applications were lacking, which made some authors question the added value of a 3D CT [14]. Reluctance to adopt 3D CTs was evident in foot and ankle literature where most available measurements and reference angels were still performed in 2D [8, 9, 15]. Nevertheless, the orthopedic field's interest in 3D printing and computer-assisted surgery (CAS) has grown in recent years [16, 17]. These tools allow for more precise preoperative planning and intraoperative surgical procedures [18]. However, in order to successfully apply them, a better understand-

Based on Burssens A, Peeters J, Peiffer M, Marien R, Lenaerts T, WBCT ISG, Vandeputte G, Victor J. Reliability and correlation analysis of computed methods to convert conventional 2D radiological hindfoot measurements to a 3D setting using weight bearing CT. *Int J Comp Assisted Radiol Surg* 2018;13(12): 1999–2008 [50].

M. Richter et al., *Weight Bearing Cone Beam Computed Tomography (WBCT) in the Foot and Ankle*, https://doi.org/10.1007/978-3-030-31949-6_10

ing of 3D technology is required. Although the application of these techniques on the skeletal system is generally well understood, their potential use on and subsequent insights from the hindfoot remain unclear; most weight-bearing research of the lower limb has been focused on hip and knee joints [19–21].

The advantage of these methods is that they incorporate each plane according to the region of interest with a high measurement accuracy [19].

Using WBCT, the previously described hindfoot measurements allow for correct foot positioning in the coronal, sagittal, and axial plane, but the actual angles are only obtained from one CT slice in one plane [7, 10, 22, 23].

Although interobserver reliability is high, important spatial data is not used, and the manually drawn angles and foot positioning steps impose additional measurement errors [8].

The aim of this paper is therefore to use computed methods to convert these conventional 2D measurements to a 3D environment. This analytic process will be assessed by rater reliability and regression analysis.

Materials and Methods

Study Population, Design, and Measurement Protocol

Forty-eight patients with clinical and radiological absence of hindfoot pathology were included [24]. The mean age was 39.6 years (SD = 3.2, age range: 19–72 years). The indications for imaging using WBCT were one of the following: minor foot and ankle trauma (e.g., foot and ankle sprain or contusion) with persistent complaints that were negative or nonsignificant for an occult fracture (n = 31), the suspicion of osteoarthritis that was undetectable on CT slices (n = 11), or a MTP I fusion to assess consolidation (n = 4) as shown in Table 10.1.

The contralateral unaffected foot was used for each analysis. The measurements were performed on the images retrieved from the weight bearing pedCAT® cone beam CT, using the incorporated Cubevue® software for the 2D analysis (CurveBeam, Warrington, PA, USA). The 3D analysis was obtained after segmentation of the images using Mimics® 19.0 and analysis using 3-matic® software (Materialise, Leuven, Belgium). The patient records were anonymized and deidentified prior to processing in accordance with the standard data release procedures of the hospital involved in the study. All procedures performed in studies involving human participants were in accordance with the ethical standards of the institutional

Table 10.1 Patient characteristics

Characteristic	Total (N = 48)
Age (±) SD	39.6 ± 13.2 years
Sex (M/F)	28/20
Minor trauma	31
Absence osteoarthritis	11
MTP I fusion	4

and/or national research committee and with the 1964 Helsinki declaration and its later amendments or comparable ethical standards. The Institutional Review Board of AZ Monica approved this study (OG10601102015), and formal consent was not required for this type of study. The following imaging protocol was used: radiation source was set at 4 mAs and 50 kV, with a focus distance of 100 cm, and the beam pointed at the ankle joint. PedCAT used the following settings: tube voltage, 96 kV; tube current, 7.5 mAs; CTDIvol 4.3 mGy; matrix, 160,160,130; pixel size, 0.4 mm; and slice interval, 0.4 mm.

At the department of radiology, patients were asked to stand naturally with both feet parallel to each other, shoulder width apart. Hindfoot measurements were performed in 2D by authors AB and MP. Each measurement was repeated three times. After the set of measurements was complete, the average of these three measurements was used for further analysis. A similar test/retest methodology was performed in other studies concerning hindfoot measurements [3, 5, 8, 25–27]. The hindfoot angle was determined based on the inferior point of the calcaneus (HA2D), as described previously [8]. In brief, the foot was first positioned in line with the collinear axis of the shaft of the second metatarsal, which is considered as the longitudinal axis of the foot in the axial plane (Fig. 10.1). The hindfoot angle was

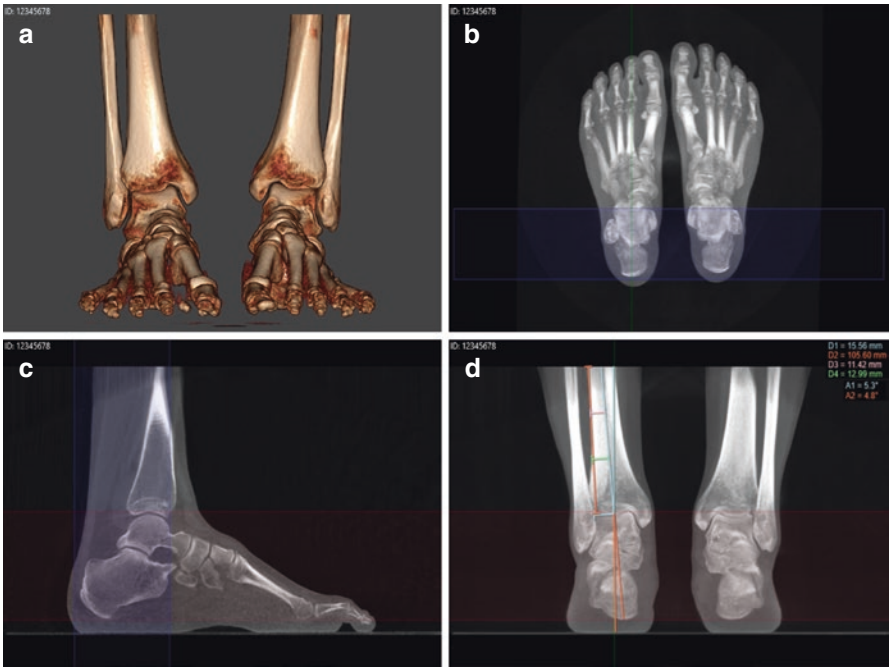

Fig. 10.1 Measuring hindfoot alignment in 2D. (**a**, **b**) Positioning of the foot in line with the axis of the second metatarsal in the axial plane. (**c**, **d**) The hindfoot angle (HA2D) is composed out of the intersection between the anatomical tibia axis (TA2D, blue line) and the talocalcaneal axis (TC2D, orange line). The TC2D connects the inferior point of the calcaneus with the middle of the talar dome

defined as the intersection between the anatomical tibia axis (TA2D) and the talocalcaneal axis (TC2D), which connects the inferior point of the calcaneus and the middle of the upper surface of the talus in the coronal plane (Fig. 10.1c, d).

The varus and valgus alignment of the hindfoot was respectively defined as when the TCA runs medial from the vertical axis and when the TCA runs lateral from the vertical axis, which is often considered as a reference axis [28, 29]. Authors RM and TL determined the 3D hindfoot angle (HA3D) by the use of computer-aided design (CAD) operations (Fig. 10.2a–d).

The anatomical tibia axis (TA3D) was calculated by a best fit centroidal axis along the diaphysis marked above the incisura fibularis (Fig. 10.2a). The talocalcaneal axis (TC3D) was computed by connecting the inferior calcaneus point (ICP) with central talus point (CTP). The ICP was obtained after the calculation of an extrema analysis of the calcaneus (function to determine the most outer point of a structure in the direction of a given axis) (Fig. 10.2b). The CTP was determined by the calculated centroid of the talus (mean position of all the points in a given structure) (Fig. 10.2c). The computed intersection of both the TA3D and the TC3D

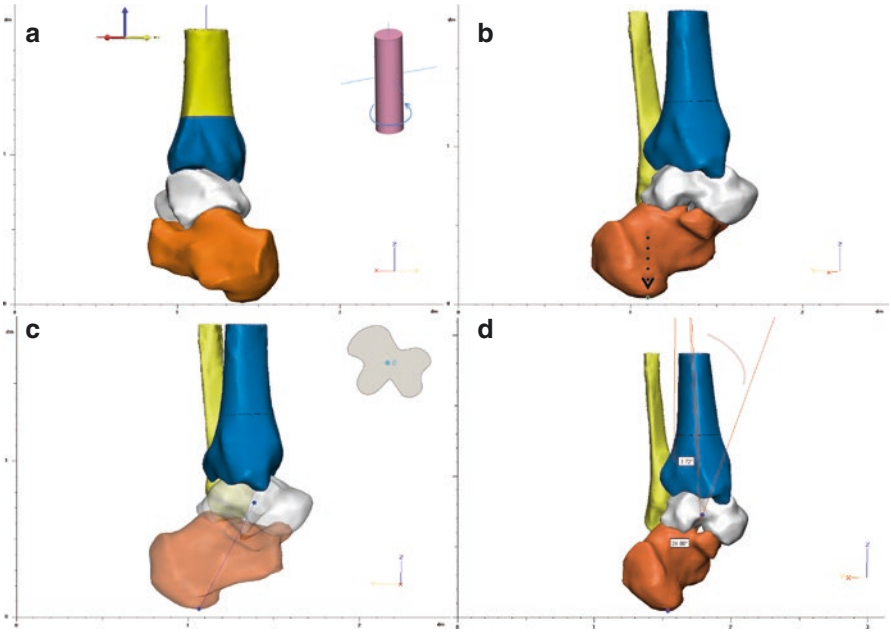

Fig. 10.2 Measuring hindfoot alignment in 3D. (**a**) The anatomical tibia axis (TA3D) was computer calculated as an axis based on the moment of inertia (depicted in the upper right quadrant) through the distal end of the tibia marked above the fibular groove. (**b**) The inferior calcaneus point was calculated by an extrema analysis (a software function to determine the most outer point in the superior-inferior direction) (arrow). (**c**) The center of the talus was calculated as a centroid (depicted in the upper right quadrant) based on the mean position of all points in the talus. The talocalcaneal axis (TC3D) was calculated by connecting the inferior calcaneus point with the centroid of the talus. (**d**) The intersection of both axes became the HA3D

became the HA3D (Fig. 10.2d). The TA and the TC were measured separately in the hindfoot angle when comparing the 2D and the 3D angles in order to emphasize possible inconsistencies attributable to either the tibial or talocalcaneal component.

The talocrural angle (TCr) was used as a radiographic parameter to assess the ankle in the coronal plane [30]. TCr was measured in 2D (TCr2D) as the angle between the intersection of the intermalleolar axis (obtained after connecting the interior point of the medial with the most inferior point of the lateral malleolus) and the horizontal axis of tibial joint line (Fig 10.3a).

In 3D (TCr3D), this measurement is performed in the same manner by the intersecting angle of the intermalleolar axis (the most inferior points of the malleoli were computed using an extrema analysis) and the computed best fitted axis through the horizontal contour of the tibial joint line (Fig. 10.3b).

Characteristics in the tibiotalar joint were measured as the inclination of the tibial joint surface towards the vertical axis perpendicular to the floor (TI2D) and the tilt of the talus towards the vertical axis perpendicular to the floor (TT2D) as described previously (Fig. 10.3c) [8].

The TI3D and TT3D were similarly analyzed by reconstructing the joint surface respective of the tibia and the talus in the coronal plane. This reconstruction allows for the computation of the horizontal axis of both surfaces and the intersection with the vertical axis perpendicular to the floor resulted in the TI3D and TT3D.

In the subtalar joint (STJ), the middle subtalar vertical angle (SVA2D) was determined in the coronal plane according to the method described by Colin et al. [9]. This measurement required the length of the posterior facet of the STJ to be measured in

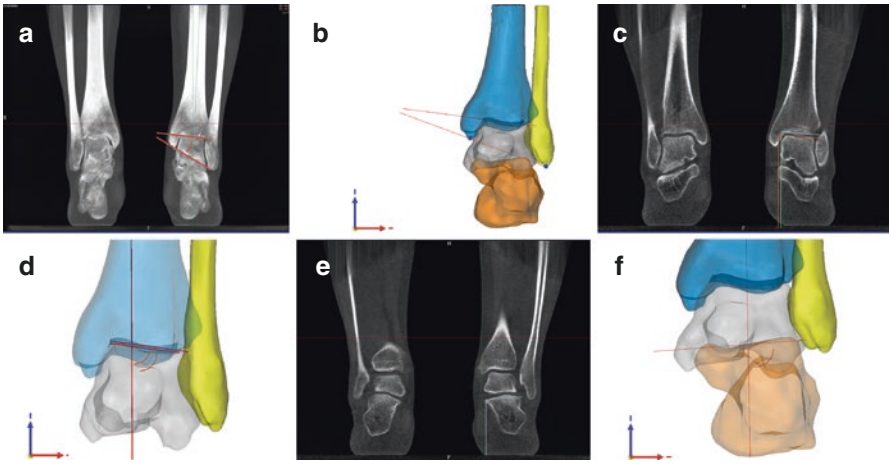

Fig. 10.3 Common ankle and hindfoot measurements. (**a**, **b**) The talocrural angle (TCr) was measured in 2D (TCr2D) by the intersection of the malleolar axis and the tibial joint line. The 3D (TCr3D) was measured as the intersection between the malleolar axis, created by connecting the inferior medial and lateral malleolus through an extremity analysis and the tibial joint line. (**c**) Characteristics in the tibiotalar joint were measured as the tibial inclination (TI2D, upper line) the talar tilt (TT2D, lower line). (**d**) Representation of the TI3D, TT3D. (**e**) Characteristics in the hindfoot were measured as the SVA (SVA 2D). (**f**) Representation of the SVA3D

the sagittal plane. In the midpoint of this distance, the inclination of the STJ surface towards the vertical axis perpendicular to the floor in the coronal plane was determined (Fig. 10.3e). The SVA3D was analyzed similarly to the SVA2D with the same methods as applied in the TI3D and TT3D, which is generalized in Fig. 10.3f and detailed in Fig. 10.4.

By applying goniometric functions built into the software, commonly used measurements from a 2D radiograph can be translated into a 3D angle and its subsequent projection. The general sequence is depicted and explained for the talocrural angle as an example (Fig. 10.4a–d).

The coronal plane in these methods was derived from the Cartesian coordinate system with the inferior calcaneus point as the origin. The *z*-axis was defined as running through the origin perpendicular to the ground floor. The *x*-axis runs through the origin perpendicular to the *z*-axis and lies in the sagittal plane, formed through the center of the second metatarsal head and the origin perpendicular to the ground floor. The *y*-axis goes through the origin, perpendicular to the *x*-axis and *z*-axis (Fig. 10.5e–f).

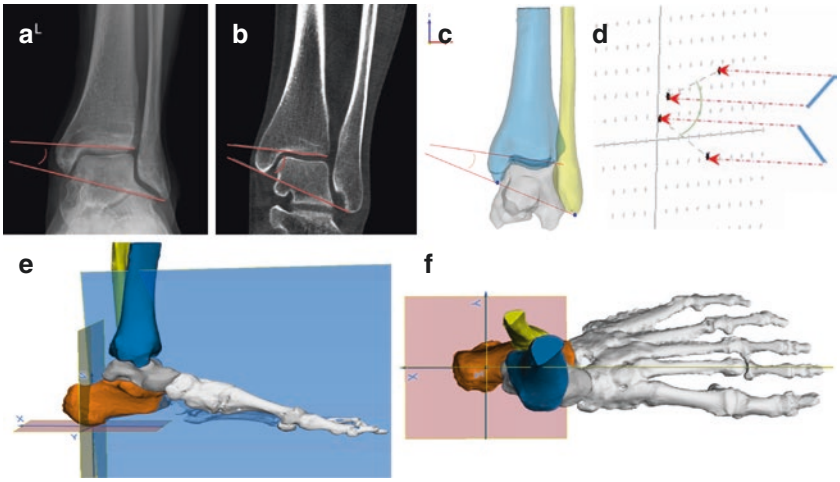

Fig. 10.4 Sequence of translating commonly used 2D measurements to 3D angles. (**a**) Starting as an example with an AP radiograph of the talocrural angle, which was measured as the intersection between the axis connecting both malleoli and the axis parallel to articular surface of the distal tibia in 2D. (**b**) Same measurement in 2D is applied by the use of weight bearing CT after correct rotation. (**c**) Computer-calculated points (blue) to determine the axes and 3D angle. (**d**) Schematic representation of projecting a 3D angle in the coronal (*yz*-plane) through the used software by applying build-in goniometric functions. (**e–f**) Cartesian coordinate system with the origin defined in the inferior point of the calcaneus. The *z*-axis was calculated perpendicular to the floor through the origin. The *x*-axis runs through the origin perpendicular to the *z*-axis and lies in the sagittal plane, formed through the center of the second metatarsal head and the origin perpendicular to the ground floor. The *y*-axis goes through the origin, perpendicular to the *x*-axis and *z*-axis

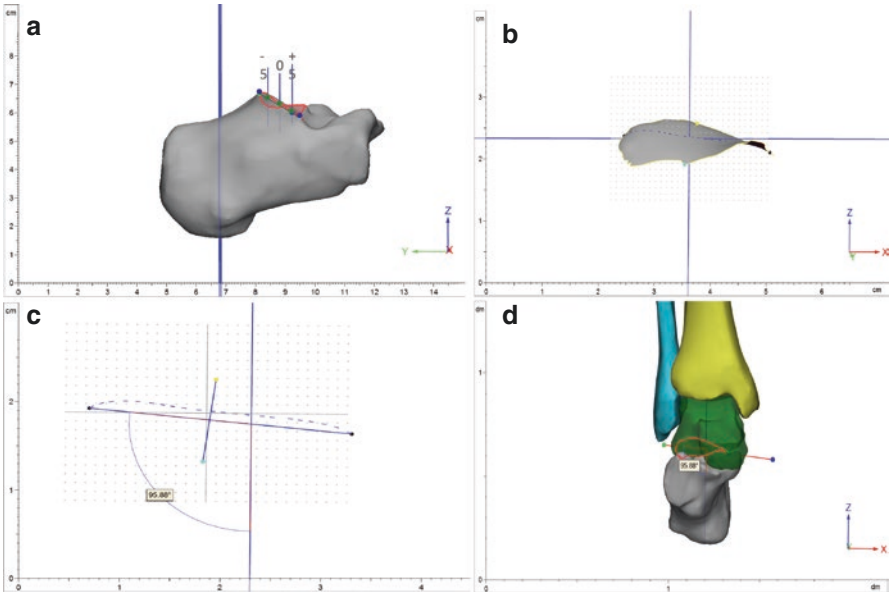

Fig. 10.5 Measurement of the subtalar vertical angle in 3D (SVA_{3D}). (**a**) The surface of the posterior facet of the subtalar joint was marked (red contour). The most posterior and anterior point of the marked surface was calculated in the direction of the AP (*x*-) axis (blue dots). This allowed to determine the length of the posterior facet by a software-operated connection of both points. The midpoint of this distance was calculated and used as an origin to fit a plane parallel to the coronal plane at a distance of −5 mm, 0 mm, and + 5 mm to mimic, respectively, the posterior, middle, and anterior SVA as described by Colin et al. [9]. (**b**) The contour of the posterior facet running in the middle subtalar plane was used to determine the inclination (dashed line) by connecting the calculated most medial with the most lateral point. (**c**) The intersection of this subtalar axis with the vertical (*z*-) axis became the middle SVA. (**d**) Depiction of the middle SVA in a 3D hindfoot configuration

Statistical Analysis

A Kolmogorov-Smirnov normality test was performed to determine if data were normally distributed. A student's t-test and Wilcoxon signed rank test were used for comparison of normally and not normally distributed data (2D vs. 3D hindfoot angles), respectively.

The correlation between the measured 2D and 3D angles was assessed by the Pearson coefficient (*r*). Linear regression analysis was demonstrated by use of a corresponding scatter plot and calculation of the r^2.

Inter- and intraobserver variability of the obtained measurements were analyzed using the interclass correlation coefficient [16]. Interpretations were as follows: ICC < 0.4, poor; 0.4 < ICC < 0.59, acceptable; 0.6 < ICC < 0.74, good; and ICC > 0.74, excellent [31].

The SPSS (release 20.0.0. standard version, SPSS, Inc., Chicago, IL, USA) statistical package was used to analyze the results. A probability level of $P < 0.05$ was considered significant.

Results

Hindfoot Alignment

The mean HA2D was 0.79° of valgus (SD = 3.2, range 12.7° of valgus–13° of varus), and the HA3D was 8.08° of valgus (SD = 6.5, range 17.2° of valgus–11.3° of varus). There was a statistically significant difference between the HA2D vs. HA3D ($P < 0.001$). There was a good correlation between both angles ($r = 0.72$, $P < 0.001$) (Fig. 10.6). The ICC3D proved to be excellent when compared to the ICC2D, which was good (Table 10.2).

The mean TA2D was 2.7° of varus (SD = 2.1, range 2.5° of valgus–9.1° of varus), and the TA3D was 5.1° of varus (SD = 4.9, range 0.68° of valgus–2.4° of varus). There was a statistically significant difference between the TA2D and TA3D ($P = 0.001$).

There was a good correlation between both angles ($r = 0.77$, $P < 0.001$) (Fig. 10.6b). The ICC2D and ICC3D were both excellent (Table 10.2).

The mean TC2D equaled 0.6° of varus (SD = 2.9, range 9.1° of valgus–12.2° of varus) and showed to be 4.6° of valgus in 3D (SD = 3.7, range 11.34° of valgus–10.71° of varus). There was a statistically significant difference between the TC2D and TC3D ($P < 0.001$). There was a good correlation between both angles ($r = 0.71$, $P < 0.001$) (Fig. 10.6c). The ICC2D and ICC3D were both excellent (Table 10.2).

Ankle and Hindfoot Characteristics

The mean TCr2D and TCr3D were 15.8° (SD = 4.7, range 10.8–23.1°) and 11.8° (SD = 3.4, range 7.2–20.71°), respectively. There was a statistically significant difference between the TCr2D and TCr3D ($P < 0.001$). There was a good correlation between both angles ($r = 0.69$, $P < 0.001$) (Fig. 10.6d). The ICC3D was excellent when compared to the ICC2D, which was good (Table 10.3).

Table 10.2 Mean hindfoot measurements in degrees and concomitant intraclass correlation coefficients

	Hindfoot measurements	SD (±)	ICC_{inter}	ICC_{intra}
HA_{2D}	0.79	3.2	0.73	0.81
TA_{2D}	2.7	2.1	0.76	0.83
TC_{2D}	0.6	2.9	0.85	0.82
HA_{3D}	8.08	6.5	0.91	0.93
TA_{3D}	5.1	4.9	0.86	0.89
TC_{3D}	4.6	3.7	0.99	0.99

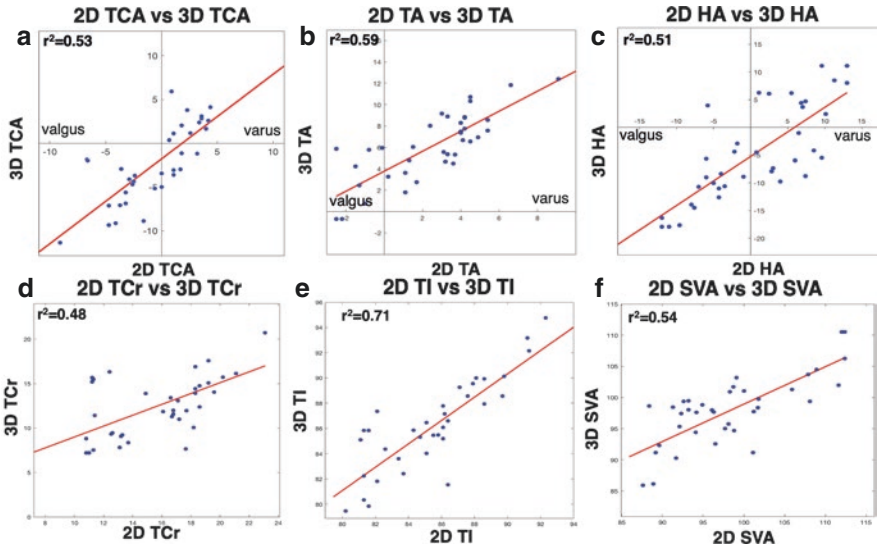

Fig. 10.6 (**a**–**f**) Correlation analysis of the conventional radiographic hindfoot characteristics measured in 2D towards the obtained 3D measurements

Table 10.3 Mean ankle and hindfoot characteristics in degrees and concomitant intraclass correlation coefficients

	Ankle/hindfoot measurements	SD (±)	ICC_{inter}	ICC_{intra}
TCr_{2D}	15.8	4.7	0.69	0.73
TI_{2D}	87.6	3.9	0.81	0.86
TT_{2D}	88.1	3.1	0.83	0.82
SVA_{2D}	96.1	5.7	0.73	0.76
TCr_{3D}	11.8	3.4	0.89	0.91
TI_{3D}	86.6	5.3	0.95	0.93
TT_{3D}	87.2	3.9	0.89	0.94
SVA_{3D}	98.4	8.1	0.81	0.84

The mean TI2D and TI3D were 87.6° (SD = 3.9, range 80.2–94.2°) and 86.6° (SD = 5.3, range 79.46–94.76°), respectively. There was a statistically significant difference between the TI2D and TI3D ($P < 0.001$). There was an excellent correlation between both angles ($r = 0.83$, $P < 0.001$) (Fig. 10.6e). The ICC2D and ICC3D showed both to be excellent (Table 10.3).

The mean TT2D and TT3D were 88.1° (SD = 3.1, range 82.6–96.2°) and 87.2° (SD = 3.9, range 82.9–99.1°), respectively. There was a statistically significant difference between the TT2D and TT3D ($P < 0.001$). There was a good correlation between both angles ($r = 0.79$, $P < 0.001$). The ICC2D and ICC3D showed both to be excellent (Table 10.1).

The mean SVA2D and SVA3D were 96.1° of valgus (SD = 7.2, range 87.6–112.4° of valgus) and 98.45° valgus (SD = 5.6, range 85.9–110.5° of valgus). There was a

statistically significant difference between the SVA2D and SVA3D ($P < 0.001$). There was a good correlation between both angles ($r = 0.73$, $P < 0.001$). These angles significantly differed from each other with a ($P < 0.001$). The ICC2D and ICC3D were both excellent (Table 10.1).

Discussion

This study shows a good correlation between the HA2D and the HA3D, indicating that both angles can be used to determine hindfoot alignment. However, the HA3D overcomes the shortcomings encountered by 2D analysis such as the manual foot position according to the longitudinal axis of the second metatarsal, operator-dependent measurements, and projection of the bony hindfoot structures solely in the coronal plane [8]. The latter imposes a loss of important spatial information such as the shape of the calcaneus, which has been demonstrated to contribute to the form or deformity of the hindfoot [32].

In our study, the HA3D was significantly higher than the HA2D. More spatial volume data and variations in the positions of the bony structures, e.g., calcaneal talar rotation, can partially explain these differences [33].

The extent that one measurement method is more accurate than the other remains a subject of debate. Since the HA_{3D} takes into account more data on volume position, it may represent the anatomy more accurately when comparing non-weight bearing with weight bearing hindfoot angles [7].

The main advantage of using the HA3D is its reproducibility, as shown by the excellent to almost perfect intraclass correlation coefficients. High ICC values can be attributed to the computer-aided design operations, which allowed for calculation of the best fitted centroidal axis of the tibia base, the most inferior point of the calcaneus, and the centroid of the talus. Each calculation was repeated according to the same mathematical algorithm, allowing for less user interference compared to other studies [19, 34]. The only user-dependent aspect in determining the hindfoot angle was marking the distal end of the tibia to determine the TA3D. This resulted in a lower ICC when compared to the TC3D. Nevertheless, reliability coefficients of the TA3D were still higher than the TA2D, and reliable landmarks were used based on previous literature [35].

These findings were also observed in other hindfoot and ankle measurements, in which complete computer-calculated angles, such as the talocrural angle, have a higher reliability than angles requiring additional surface analysis such as the TT, TI, and SVA. On the other hand, the talocrural angle showed a lower correlation between 2D and 3D analysis due to the 2D CT measurement difficulties; in a 2D CT, the fibula and the tibia do not lie in the same coronal plane but are angulated 20–30° towards each other [36].

This suggests that obtaining 3D volume data allows for a better multiplanar insight, which is often required in clinical practice during foot and ankle surgery [37].

Another important factor that could influence the obtained measurements is the process of manually segmenting CT slices to obtain volumes. However, these methods have been shown to have a high accuracy in CT, CBCT, and MRI [38–40]. Recent developments even allow fully automatic segmentation of long bones [34, 41].

The limitation of using only the distal part of the tibia in determining the hindfoot alignment could contribute to the higher variation in tibia measurements and is a general limitation of this study. Stufkens et al. [42] confirmed these variations by the marked difference in the medial distal tibia angle (MDTA) measured on whole lower limb radiographs compared to the MDTA in mortise radiographs of the ankle. If the cone beam gantry could scan the entire tibia, more accurate measurements could be obtained as pointed out by Victor et al. [43]. Another method to determine hindfoot alignment overcomes this problem by using the forefoot as a reference based on the tripod index [44, 45]. Recently, Lintz et al. [46] pointed the efficiency out of this 3D biometric tool as part of the TALAS system. For both 3D methods, the radiation dose remains the same and should be taken into account. When compared to plane radiographs, this method is the equivalent of six radiographs for a unilateral PedCAT cone beam CT and 5.6% of the dose from a classic foot and ankle CT [7, 47].

In conclusion, this study shows that 3D measurement methods are more accurate and reproducible than 2D methods. The technique is based on previously described plane radiographs and CT measurements, which makes the interpretation and use for clinical practice straightforward [2, 7, 8]. It should be taken into account that all new 3D measurements cannot be compared to previous measurements and should therefore be firstly evaluated in future radiological and clinical studies, before any strong suggestions and guidelines can be made. The main advantage in clinical practice can be appertained to an improved understanding of complex hindfoot pathology by the provided 3D structural configuration in WBCT. Future research and clinical applications could therefore apply this measurement method in patients with a significant malalignment of the hindfoot. This will provide more preoperative insights into the multiplanar deformity, to facilitate the preoperative surgical planning of the correction, which is currently based on 2D measurements as pointed out by Barg et al. [48] Computer-assisted surgical techniques could incorporate the obtained 3D reference values per-operatively to help corrections of malaligned hindfoot fall within normal angular parameters, as shown by Richter et al. [17]. Postoperative assessment of the achieved correction by the same 3D measurement methods will provide a better quantification and understanding of the surgical intervention.

These findings will prompt more evidence-based surgery and better treatment guidelines. The latter are currently incoherent, reflecting the lack of structural insight into hindfoot pathology [49].

Acknowledgments The authors wish to thank Ir. Karim Chellaoui, as a clinical engineer for his attributive remarks to the study design and thorough review of the statistics.

The linguistic and structural support was provided by Maxwell Weinberg, research assistant at the University of Utah and Hannes Van Wynendaele, MLing of Ugent.

References

1. Cobey JC. Posterior roentgenogram of the foot. Clin Orthop Relat Res. 1976;118:202–7.
2. Saltzman CL, El-Khoury GY. The hindfoot alignment view. Foot Ankle Int. 1995;16(9):572–6.
3. Reilingh ML, Beimers L, Tuijthof GJM, Stufkens SAS, Maas M, van Dijk CN. Measuring hindfoot alignment radiographically: the long axial view is more reliable than the hindfoot alignment view. Skelet Radiol. 2010;39(11):1103–8.
4. Buck FM, Hoffmann A, Mamisch-Saupe N, Espinosa N, Resnick D, Hodler J. Hindfoot alignment measurements: rotation-stability of measurement techniques on hindfoot alignment view and long axial view radiographs. Am J Roentgenol. 2011;197(3):578–82.
5. Barg A, Amendola RL, Henninger HB, Kapron AL, Saltzman CL, Anderson AE. Influence of ankle position and radiographic projection angle on measurement of supramalleolar alignment on the anteroposterior and hindfoot alignment views. Foot Ankle Int. 2011;36(11):1352–61.
6. Ikoma K, Noguchi M, Nagasawa K, Maki M, Kido M, Hara Y, Kubo T. A new radiographic view of the hindfoot. J Foot Ankle Res. 2013;6(1):48.
7. Richter M, Seidl B, Zech S, Hahn S. PedCAT for 3D-imaging in standing position allows for more accurate bone position (angle) measurement than radiographs or CT. Foot Ankle Surg. 2014;20(3):201–7.
8. Burssens A, Peeters J, Buedts K, Victor J, Vandeputte G. Measuring hindfoot alignment in weight bearing CT: a novel clinical relevant measurement method. Foot Ankle Surg. 2011;22(4):233–8.
9. Colin F, Lang TH, Zwicky L, Hintermann B, Knupp M. Subtalar joint configuration on weight-bearing CT scan. Foot Ankle Int. 2014;35(10):1057–62. 1071100714540890.
10. Krähenbühl N, Tschuck M, Bolliger L, Hintermann B, Knupp M. Orientation of the subtalar joint measurement and reliability using weightbearing CT scans. Foot Ankle Int. 2016;37(1):109–14.
11. Tuominen EK, Kankare J, Koskinen SK, Mattila KT. Weight-bearing CT imaging of the lower extremity. AJR Am J Roentgenol. 2013;200(1):146–8.
12. O'Connor JF, Cohen J. Computerized tomography (CAT scan, CT scan) in orthopaedic surgery. J Bone Joint Surg Am. 1978;60(8):1096–8.
13. Wicky S, Blaser P, Blanc C, Leyvraz P, Schnyder P, Meuli R. Comparison between standard radiography and spiral CT with 3D reconstruction in the evaluation, classification and management of tibial plateau fractures. Eur Radiol. 2000;10(8):1227–32.
14. te Stroet MA, Holla M, Biert J, van Kampen A. The value of a CT scan compared to plain radiographs for the classification and treatment plan in tibial plateau fractures. Emerg Radiol. 2011;18(4):279–83.
15. Sanders R. Current concepts review-displaced intra-articular fractures of the calcaneus. J Bone Joint Surg. 2000;82(2):225–50.
16. Auricchio F, Marconi S. 3D printing: clinical applications in orthopaedics and traumatology. EFORT Open Rev. 2016;1(5):121–7.
17. Richter M. Computer aided surgery in foot and ankle: applications and perspectives. Int Orthop. 2013;37(9):1737–45.
18. Tack P, Victor J, Gemmel P, Annemans L. 3D-printing techniques in a medical setting: a systematic literature review. Biomed Eng Online. 2016;15(1):115.
19. Jacxsens M, Van Tongel A, Willemot LB, Mueller AM, Valderrabano V, De Wilde L. Accuracy of the glenohumeral subluxation index in nonpathologic shoulders. J Shoulder Elbow Surg. 2015;24(4):541–6.
20. Victor J, Premanathan A. Virtual 3D planning and patient specific surgical guides for osteotomies around the knee. Bone Joint J. 2013;95(11 Supple A):153–8.
21. Audenaert EA, Baelde N, Huysse W, Vigneron L, Pattyn C. Development of a three-dimensional detection method of cam deformities in femoroacetabular impingement. Skelet Radiol. 2011;40(7):921–7.

22. Hirschmann A, Pfirrmann CWA, Klammer G, Espinosa N, Buck FM. Upright cone CT of the hindfoot: comparison of the non-weight-bearing with the upright weight-bearing position. Eur Radiol. 2013;24(3):553–8.
23. de Cesar Netto C, Schon LC, Thawait GK, da Fonseca LF, Chinanuvathana A, Zbijewski WB, Siewerdsen JH, Demehri S. Flexible adult acquired flatfoot deformity: comparison between weight-bearing and non-weight-bearing measurements using cone-beam computed tomography. J Bone Joint Surg. 2017;99(18):e98.
24. Burssens A, Van Herzele E, Buedts K, Leenders T, Clockaerts S, Vandeputte G, Victor J. Weightbearing CT in normal hindfoot alignment – presence of constitutional valgus? Foot Ankle Surg. 2017;23:16.
25. Barg A, Harris MD, Henninger HB, Amendola RL, Saltzman CL, Hintermann B, Anderson AE. Medial distal tibial angle: comparison between weightbearing mortise view and hindfoot alignment view. Foot Ankle Int. 2012;33(8):655–61.
26. Neri T, Barthelemy R, Tourné Y. Radiologic analysis of hindfoot alignment: comparison of Méary, long axial, and hindfoot alignment views. Orthop Traumatol Surg Res. 2017;103(8):1211–6.
27. Dagneaux L, Moroney P, Maestro M. Reliability of hindfoot alignment measurements from standard radiographs using the methods of Meary and Saltzman. Foot Ankle Surg. 2019;25(2):237–41.
28. Iseki Y, Takahashi T, Takeda H, Tsuboi I, Imai H, Mashima N, Watanabe S, Yamamoto H. Defining the load bearing axis of the lower extremity obtained from anterior-posterior digital radiographs of the whole limb in stance. Osteoarthr Cartil. 2009;17(5):586–91.
29. Guichet J-M, Javed A, Russell J, Saleh M. Effect of the foot on the mechanical alignment of the lower limbs. Clin Orthop Relat Res. 2009;415:193–201.
30. Brage ME, Bennett CR, Whitehurst JB, Getty PJ, Toledano A. Observer reliability in ankle radiographic measurements. Foot Ankle Int. 1997;18(6):324–9.
31. Shrout PE, Fleiss JL. Intraclass correlations: uses in assessing rater reliability. Psychol Bull. 1979;86(2):420.
32. Hamel J. Calcaneal Z osteotomy for correction of subtalar hindfoot varus deformity. Oper Orthop Traumatol. 2015;27(4):308.
33. Lundberg A, Svensson O. The axes of rotation of the talocalcaneal and talonavicular joints. Foot. 1993;3(2):65–70.
34. Almeida DF, Ruben RB, Folgado J, Fernandes PR, Audenaert E, Verhegghe B, De Beule M. Fully automatic segmentation of femurs with medullary canal definition in high and in low resolution CT scans. Med Eng Phys. 2016;38(12):1474–80.
35. Chen Y, Qiang M, Zhang K, Li H, Dai H. A reliable radiographic measurement for evaluation of normal distal tibiofibular syndesmosis: a multi-detector computed tomography study in adults. J Foot Ankle Res. 2015;8(1):1.
36. Hansen M, Le L, Wertheimer S, Meyer E, Haut R. Syndesmosis fixation: analysis of shear stress via axial load on 3.5-mm and 4.5-mm quadricortical syndesmotic screws. J Foot Ankle Surg. 2006;45(2):65–9.
37. Quill GE. Reconstruction of multiplanar ankle and hindfoot deformity with intramedullary techniques. Foot Ankle Clin. 2009;14(3):533–47.
38. Van den Broeck J, Vereecke E, Wirix-Speetjens R, Vander Sloten J. Segmentation accuracy of long bones. Med Eng Phys. 2014;36(7):949–53.
39. Al-Rawi B, Hassan B, Vandenberge B, Jacobs R. Accuracy assessment of three-dimensional surface reconstructions of teeth from cone beam computed tomography scans. J Oral Rehabil. 2010;37(5):352–8.
40. Rathnayaka K, Sahama T, Schuetz MA, Schmutz B. Effects of CT image segmentation methods on the accuracy of long bone 3D reconstructions. Med Eng Phys. 2011;33(2):226–33.
41. Ebinger T, Goetz J, Dolan L, Phisitkul P. 3D model analysis of existing CT syndesmosis measurements. Iowa Orthop J. 2013;33:40.

42. Stufkens SA, Barg A, Bolliger L, Stucinskas J, Knupp M, Hintermann B. Measurement of the medial distal tibial angle. Foot Ankle Int. 2011;32(3):288–93.
43. Victor J, Van Doninck D, Labey L, Van Glabbeek F, Parizel P, Bellemans J. A common reference frame for describing rotation of the distal femur. Bone Joint J. 2009;91(5):683–90.
44. Lintz F, Barton T, Millet M, Harries WJ, Hepple S, Winson IG. Ground reaction force calcaneal offset: a new measurement of hindfoot alignment. Foot Ankle Surg. 2012;18(1):9–14.
45. Arunakul M, Amendola A, Gao Y, Goetz JE, Femino JE, Phisitkul P. Tripod index: a new radiographic parameter assessing foot alignment. Foot Ankle Int. 2013;34(10):1411–20.
46. Lintz F, Welck M, Bernasconi A, Thornton J, Cullen NP, Singh D, Goldberg A. 3D biometrics for Hindfoot alignment using weightbearing CT. Foot Ank Int. 2017;38(6):684–9.1071100717690806.
47. Ludlow JB, Ivanovic M. Weightbearing CBCT, MDCT, and 2D imaging dosimetry of the foot and ankle. Int J Diagn Imaging. 2014;1(2):1.
48. Barg A, Saltzman CL. Single-stage supramalleolar osteotomy for coronal plane deformity. Curr Rev Musculoskelet Med. 2014;7(4):277–91.
49. Van Gestel L, Van Bouwel S, Somville J. Surgical treatment of the adult acquired flexible flatfoot. Acta Orthop Belg. 2015;81(2):172–83.
50. Burssens A, Peeters J, Peiffer M, Marien R, Lenaerts T, WBCT ISG, Vandeputte G, Victor J. Reliability and correlation analysis of computed methods to convert conventional 2D radiological hindfoot measurements to a 3D setting using weight bearing CT. Int J Comp Assisted Radiol Surg. 2018;13(12):1999–2008.